

Effect of grading pattern and porosity on the eigen characteristics of porous functionally graded structure

Prashik Malhari Ramteke¹, Subrata K. Panda*¹ and Nitin Sharma²

¹ Department of Mechanical Engineering, NIT Rourkela, Rourkela-769008, Sundergarh, Odisha, India

² School of Mechanical Engineering, KIIT Bhubaneswar, Bhubaneswar-751024, Odisha, India

(Received August 9, 2019, Revised November 7, 2019, Accepted November 19, 2019)

Abstract. The current article proposed to develop a geometrical model for the analysis and modelling of the uniaxial functionally graded structure using the higher-order displacement kinematics with and without the presence of porosity including the distribution. Additionally, the formulation is capable of modelling three different kinds of grading patterns i.e., Power-law, sigmoid and exponential distribution of the individual constituents through the thickness direction. Also, the model includes the distribution of porosity (even and uneven kind) through the panel thickness. The structural governing equation of the porous graded structure is obtained (Hamilton's principle) and solved mathematically by means of the isoparametric finite element technique. Initially, the linear frequency parameters are obtained for different geometrical configuration via own computer code. The comparison and the corresponding convergence studies are performed for the unidirectional FG structure for the validation purpose. Finally, the impact of different influencing parameters like aspect ratio (O), thickness ratio (S), curvature ratio (R/h), porosity index (λ), type of porosity (even or uneven), power-law exponent (n), boundary condition on the free vibration characteristics are obtained for the FG panel and discussed in details.

Keywords: functionally graded materials; porosity; grading pattern; higher-order shear deformation theory; effective material properties

1. Introduction

Functionally graded material (FGM) have attracted the researchers because of its customized properties. This material has been created by taking the continuous variation of individual volume fractions of the ceramic and metal components in an effective way to fit the necessity of engineering structure. The design and analysis of graded structure not only important but also challenging. The increase in the application of FGM attracts different material researcher and the design engineers for their complete understanding. Moreover, to achieve the proper distribution of material constituent always a challenge and the research also focuses on different grading patterns (Chi and Chung 2006) i.e., power-law distribution graded material (P-FGM), exponential grading (E-FGM) and sigmoid type of grading (S-FGM). To achieve the desired kind of graded material, the component follows various fabrication techniques (Jamaludin *et al.* 2013). Out of the available techniques of preparation, the sintering of different volume fractions of individual constituents is poured into the desired shape of the die, which, in turn, may

induce the porosity within the part component. The porosity may reduce the structural strength/stiffness and the subsequent performances. In general, porosity within the structural component can be modelled by considering their distribution type (Wang and Zu 2017) i.e., even and uneven type.

To understand the current developments in the field of porous FG structure under the influence of the grading patterns, directional dependence of grading and geometrical configurations, a few relevant literatures are discussed in the following lines. In this regard, the eigenvalue solutions i.e., the free vibration and buckling load parameters of S-FGM shell structure reported by Han *et al.* (2008) assuming the constant Poisson ratio. The structural model and their corresponding responses largely depend on the type of kinematic models, it majorly represents the structural displacement and the continuity condition of the stress/strain. Hence, the researchers have made a number of efforts in the past to count the exact mid-plane kinematics for the layered composite and graded structures. In this line, the first-order and higher-order shear deformation theories (FSDT and HSDT) have received huge attention for structural modelling and analysis. The FSDT kinematics has been utilized by various researcher (Tornabene 2009 and Thai and Choi 2013) for the evaluation of dynamic deformation characteristics, the free vibration frequency and the static deflection of the FG thick/thin plate structure whereas Vu *et al.* (2017) used same kinematic model with four-variable refined plate theory for the free vibration and static bending analyse. Also, the higher-order kinematic

*Corresponding author, Ph.D., Associate Professor,
E-mail: call2subrat@gmail.com; pandask@nitrkl.ac.in

^a Lead author, M. Tech, Research Scholar
E-mail: prashikramteke793@gmail.com

^b Co-author, Ph.D., Assistant Professor,
E-mail: nits.iiit@gmail.com

model (HSDT) has been adopted to evaluate various structural responses i.e., the modal frequency and static deflection parameters of the FG structural components by Atmane *et al.* (2010) including two grading patterns (P-FGM and E-FGM), whereas the responses of the P-FGM grading effect discussed in Talha and Singh (2010). Moreover, the buckling load and the natural frequency data obtained by Meiche *et al.* (2011) for the FG sandwich thick plate structure considering the transverse shear deformation effects. Mohammadi and Ghannadpour (2011) presented the accurate vibration solutions of the nano Timoshenko beams by using Eringen's nonlocal elasticity theory while Ghassabi *et al.* (2017) presented the impact of scale factor on the frequency characteristics of FG nanoplate structure by utilizing the nonlocal elasticity theory. Similarly, the third-order plate theory adopted to investigate the free vibration frequency of the cracked FG thick rectangular plates by Huang *et al.* (2011) whereas the same kinematic model utilized to compute the analytical solutions of the free vibration, static bending and buckling responses by Kim and Reddy (2013). Wattanasakulpong *et al.* (2012) investigated the fabrication of the layered FG beam component and the corresponding experimental modal data. The vibration, bending and buckling analysis of the nonlocal Euler beams (Ghannadpour *et al.* 2013) and FG plate (Vu *et al.* 2019) performed by employing the Ritz method and sin shear deformation plate theory in association with the effective meshfree method, respectively. Hebali *et al.* (2014) used a newly developed quasi-three-dimensional (3D) hyperbolic shear deformation theory to obtain the free vibration and bending behaviour of the FG plates. Asadi *et al.* (2014) evaluated vibration responses of the internal line supported FG plates subjected to in-plane static forces. The free vibration analysis of FG beams presented by Mashat *et al.* (2014) using Carrera Unified Formulation (CUF) and by solving governing equations with the help of the principle of Virtual Displacement. Also, Kirchhoff's plate theory utilized by Chakraverty and Pradhan (2014) for the computation of the modal responses of the rectangular FG plates under the influence of different end boundary conditions. Similarly, the infinitesimal elasticity theory and the analytical formulation adopted by Ghannad and Gharooni (2012) in the HSDT kinematics for the analysis of the thick-walled axisymmetric FG cylinders under the internal and/or external pressure. The numerical frequencies and the corresponding mode shapes of the FGM plate under the different end constraints investigated by Ramu and Mohanty (2014) via the finite element method (FEM). Belkorissat *et al.* (2015) employed a new nonlocal hyperbolic refined plate model to compute the Eigen characteristics of the FG plate. An efficient technique based on unidirectional beam finite element analysis (FEA) was developed by Sheikh *et al.* (2015) for the vibration analysis of thin-walled laminated composite beams. Arani and Kolahchi (2016) obtained the nonlinear transverse vibrations of an embedded piezoelectric plate rested on Pasternak foundation with carbon nanotubes reinforcement by employing differential quadrature method (DQM). The large-amplitude flexural vibration of the uniform or FG

carbon nanotube reinforced composites plates (CNTRC) presented by Mirzaei and Kiani (2017) using a von-Karman kind of geometrical nonlinearity. Liu *et al.* (2017) used isogeometric analysis and a new non-classical FSDT to present frequency, deformation and buckling analysis of FG thick microplates. Likewise, the commercial FE package (ANSYS) has also been adopted (Bohra *et al.* 2017) to compute the natural frequency data of the FG plate structure under the influence of variable end conditions (all sides simply supported, SSSS; two sides simply-supported and remaining two sides are clamped, SSCC). The influence of skew angle on the modal responses of the cylindrical FG-CNTRC investigated (Kiani *et al.* 2018) including the distribution of CNT (uniform and non-uniform) along the thickness direction. Further, Barati and Zenkour (2018) employed FSDT and Galerkin's method to obtain the free vibration characteristics of the porous nanocomposites shells reinforced by graphene platelets. Also, the effect of reinforcement of nanoparticles including carbon nanotubes on the structural responses (frequency, dynamic, buckling and postbuckling) have been examined by Hajmohammad *et al.* (2018), Amnieh *et al.* (2018), Kolahchi *et al.* (2019) and Jassas *et al.* (2019) under the influence of ambient and elevated hostile environment (magneto-hydrothermal, hygrothermal).

It is important to discuss regarding the porosity type of defect in the FG structure majorly observed during their manufacturing process, which, in turn, affects the structural integrity and the corresponding final performances. The Vibration characteristics of the FGM doubly-curved shell panel (Jouneghani *et al.* 2017) and FG nanoplates (Shahverdi and Barati, 2017) with the effect of porosity are discussed using FSDT kinematics. Wang and Zu (2017) investigated the vibration behaviour of the FGM plates containing even and uneven porosities and moving in a thermal environment. The frequency parameters computed for the porous S-FGM plate (Wang and Zu 2018) and S-FGM beam (Avcar 2019) including von-Karman type geometrical nonlinear plate theory. The structural model in the latter case utilized two kinematic models i.e., the lower-order displacement functions (FSDT) and the classical beam theory (CBT), whereas the former study adopted the FSDT type of model. Further, the thermo-elastic vibration characteristics of the FG panels with porosity is investigated by Amir and Talha (2019) based on HSDT kinematics.

The review clearly indicates that the major study relevant to graded structure reported on P-FG kind of distribution instead of other available types. Similarly, a major study does not include the effect of porosity distribution either even or uneven type. Hence, the objective of the current study is to derive a generic type of mathematical formulation, which can include the effect of various grading patterns (power-law, exponential and sigmoid) and subsequent effect on their natural frequency parameter with and without porosity. Also, the model includes the distribution pattern of porosity i.e., even and uneven type. For this purpose, the structural responses obtained numerically using the own computer code prepared in MATLAB through the currently proposed mathematical model. The current model validity is

established via comparing the currently computed frequencies with the published data. The finite element solutions of the linear free vibration frequencies of different types of FGM including the porosity are obtained for different geometrical parameter including the porosity aspect.

2. Mathematical formulation

2.1 Effective material properties

In this section, the variation of material properties of FG panel structure along the thickness direction (X_3 -axis) is discussed including the classification. In general, the top and bottom surface ($X_3 = h/2$ and $X_3 = -h/2$) of the FG panel is assumed to be ceramic and metal-rich, respectively. Further, the elastic property variation has been obtained numerically using the available methodologies i.e., Voigt’s model (simple rule of mixture) in association with the material volume fraction along the thickness direction. In this analysis, three kinds of variation of individual constituent along the thickness direction are utilized i.e., power-law type distribution, exponential and sigmoid type with and without porosities (even and uneven).

2.1.1 P-FGM

According to the P-FGM method, variation of the material property in the thickness direction is given by (Chi and Chung 2006)

$$P = (P_c - P_m)V_{fc} + P_m \tag{1}$$

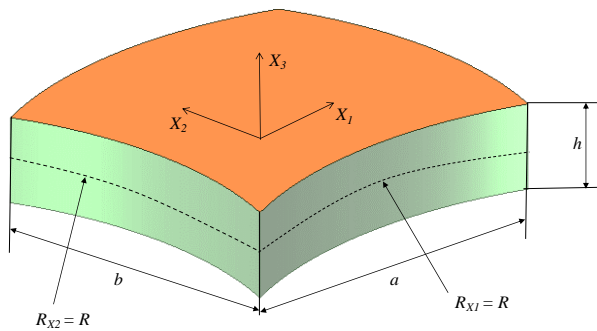


Fig. 1 FG Curved panel

The material properties of the P-FGM after introducing even and uneven porosity in Eq. (1) can be rewritten in Eqs. (2)-(3), respectively (Wang and Zu 2017). In uneven porosity distribution, the middle zone of the cross-section is rich with porosity whereas, towards the bottom and top of the cross-section, the porosity amount is decreases linearly.

$$P = (P_c - P_m)V_{fc} + P_m - 0.5\lambda \times (P_c + P_m) \tag{2}$$

$$P = (P_c - P_m)V_{fc} + P_m - 0.5\lambda \times (P_c + P_m) \left(1 - \frac{2|X_3|}{h}\right) \tag{3}$$

where, P is the effective material property of FGM in the X_3 -direction, similarly, P_c and P_m are the material properties of the ceramic and metal, respectively, X_3 is any random point in thickness direction. Additionally, the total plate thickness, porosity index and power exponent are defined as ‘ h ’, λ and n , respectively. The volume fraction of ceramic and metal are $V_{fc} = (0.5 + X_3/h)^n$ and $V_{fm} = 1 - V_{fc}$, respectively. The geometry of the FG curved panel is shown in Fig. 1 whereas the even and uneven porosity distribution pattern with material grading of the FGM is shown in Fig. 2 (Amir and Talha 2019). In addition, the variation of volume fraction of ceramic and metal according to P-FGM grading with respect to thickness ratio is shown in Fig. 3. The volume fraction of ceramic increases quickly adjacent to the bottom surface for $n < 1$ and changes rapidly adjacent to

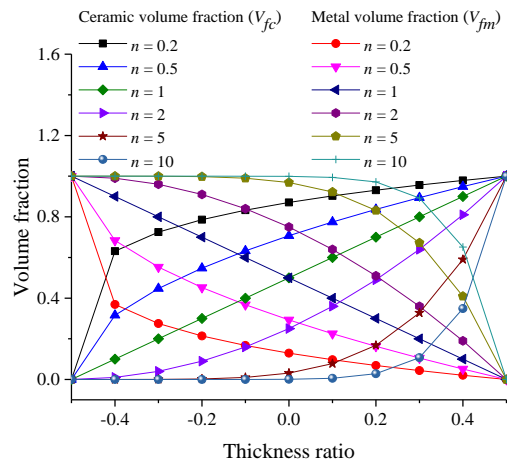
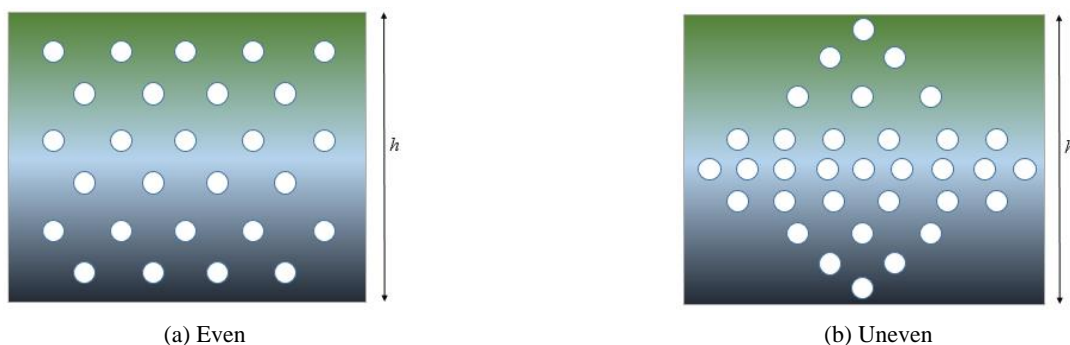


Fig. 3 Variation of volume fraction in P-FGM panel



(a) Even

(b) Uneven

Fig. 2 FG panel with even and uneven porosity distribution

the top surface for $n > 1$.

2.1.2 S-FGM

For the smooth variation of material properties, two power-law functions are utilized to define the volume fraction via the rule of mixture and presented in Eqs. (4)-(5) (Chi and Chung 2006). Similarly, the material properties of S-FGM including the porosity (even and uneven distribution) are expressed through another set of mathematical formulae similar to the source (Avcar 2019) through Eqs. (6)-(7) and Eqs. (8)-(9), respectively.

$$P = (P_c - P_m) \left[1 - 0.5 \left(1 - \frac{2X_3}{h} \right)^n \right] + P_m \text{ for } 0 \leq X_3 \leq h/2 \quad (4)$$

$$P = (P_c - P_m) \left[0.5 \left(1 + \frac{2X_3}{h} \right)^n \right] + P_m \text{ for } -h/2 \leq X_3 \leq 0 \quad (5)$$

$$P = (P_c - P_m) \left[1 - 0.5 \left(1 - \frac{2X_3}{h} \right)^n \right] + P_m - 0.5\lambda \times (P_c + P_m) \text{ for } 0 \leq X_3 \leq h/2 \quad (6)$$

$$P = (P_c - P_m) \left[0.5 \left(1 + \frac{2X_3}{h} \right)^n \right] + P_m - 0.5\lambda \times (P_c + P_m) \text{ for } -h/2 \leq X_3 \leq 0 \quad (7)$$

$$P = (P_c - P_m) \left[1 - 0.5 \left(1 - \frac{2X_3}{h} \right)^n \right] + P_m - 0.5\lambda \times (P_c + P_m) \left(1 - \frac{2|X_3|}{h} \right) \text{ for } 0 \leq X_3 \leq h/2 \quad (8)$$

$$P = (P_c - P_m) \left[0.5 \left(1 + \frac{2X_3}{h} \right)^n \right] + P_m - 0.5\lambda \times (P_c + P_m) \left(1 - \frac{2|X_3|}{h} \right) \text{ for } -h/2 \leq X_3 \leq 0 \quad (9)$$

The relation between thickness and volume fraction constituents for the S-FGM is shown in Fig. 4. It is clear from the figure that the volume fraction of ceramic and metal is same i.e., 0.5 at thickness ratio equal to zero.

2.1.3 E-FGM

The material property variation according to the exponential grading is described by Eq. (10) as follows (Chi and Chung 2006)

$$P = P_c \times e^{-\frac{1}{2} \ln\left(\frac{P_c}{P_m}\right) \left(1 - \frac{2X_3}{h}\right)} \quad (10)$$

Now, the material properties of E-FGM with two type of porosity distribution (even and uneven) obtained by Eqs. (11)-(12), respectively.

$$P = P_c \times e^{\left(-\frac{1}{2} \ln\left(\frac{P_c}{P_m}\right) \left(1 - \frac{2X_3}{h}\right) - 0.5\lambda \times \ln\left(\frac{P_c}{P_m}\right)\right)} \quad (11)$$

$$P = P_c \times e^{\left(-\frac{1}{2} \ln\left(\frac{P_c}{P_m}\right) \left(1 - \frac{2X_3}{h}\right) - 0.5\lambda \times \ln\left(\frac{P_c}{P_m}\right) \left(1 - \frac{2|X_3|}{h}\right)\right)} \quad (12)$$

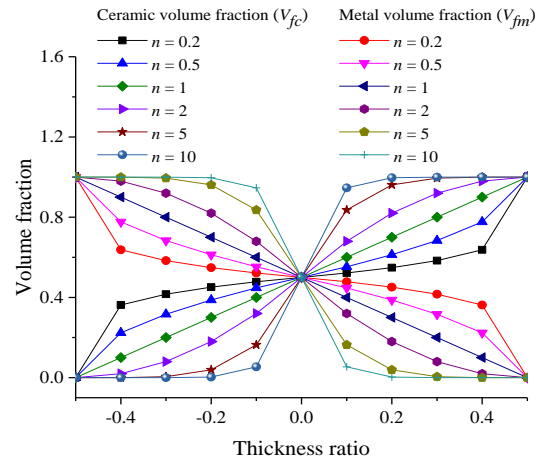


Fig. 4 Volume fraction variation in S-FGM panel

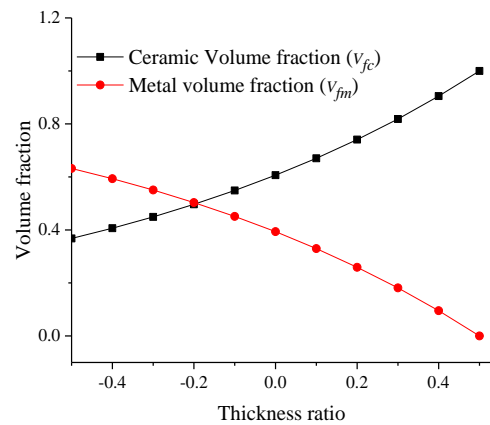


Fig. 5 Volume fraction variation in E-FGM panel

The volume fraction distribution of E-FGM for ceramic and metal constituents in the thickness direction is shown in Fig. 5.

2.2 Displacement field based on HSDT

The FGM curved panel of various geometrical dimension i.e., the total thickness ‘ h ’ along the X_3 -axis, whereas length ‘ a ’ and ‘ b ’ along the X_1 and X_2 -axis, respectively (refer Fig. 1). Further, the radii of curvatures of the panel at the mid-plane along their principal material direction specified as R_{X1} and R_{X2} , respectively. The material displacement field expressed using the HSDT as in the source (Kar and Panda 2016)

$$\left. \begin{aligned} X_{11}(X_1, X_2, X_3) &= X_{110}(X_1, X_2) + X_3\psi_x(X_1, X_2) \\ &\quad + X_3^2 X_{110}^*(X_1, X_2) + X_3^3 \psi_x^*(X_1, X_2) \\ X_{22}(X_1, X_2, X_3) &= X_{220}(X_1, X_2) + X_3\psi_y(X_1, X_2) \\ &\quad + X_3^2 X_{220}^*(X_1, X_2) + X_3^3 \psi_y^*(X_1, X_2) \\ X_{33}(X_1, X_2, X_3) &= X_{330}(X_1, X_2) \end{aligned} \right\} \quad (12)$$

where, X_{11} , X_{22} , X_{33} and X_{110} , X_{220} , X_{330} are the global and mid-plane displacement field along X_1 , X_2 , and X_3 -direction, respectively. ψ_x , ψ_y are rotations of transverse normal about X_2 , and X_1 -axis, respectively. X_{110}^* , X_{220}^* ,

ψ_x^*, ψ_y^* are the higher-order terms of Taylor's series expansion, X_3^2 and X_3^3 are the square and cubic thickness coordinates, respectively.

2.2.1 Strain-displacement relations

The strain-displacement expression for the FGM structure is represented in Green-Lagrange sense as (Reddy 2004)

$$\{\varepsilon\} = \varepsilon_l = \begin{Bmatrix} \varepsilon_{X_1 X_1} \\ \varepsilon_{X_2 X_2} \\ \gamma_{X_1 X_2} \\ \gamma_{X_1 X_3} \\ \gamma_{X_2 X_3} \end{Bmatrix} = \begin{Bmatrix} \overline{X_{11,X_1}} \\ \overline{X_{22,X_2}} \\ \overline{X_{11,X_2}} + \overline{X_{22,X_1}} \\ \overline{X_{11,X_3}} + \overline{X_{33,X_1}} \\ \overline{X_{22,X_3}} + \overline{X_{33,X_2}} \end{Bmatrix} \quad (14)$$

where, ε_l is linear strain tensors

$$\begin{aligned} \overline{X_{11,X_1}} &= \frac{\partial X_{11}}{\partial X_1} + \frac{X_{33}}{R_{X_1}}; \\ \overline{X_{11,X_2}} &= \frac{\partial X_{11}}{\partial X_2}; & \overline{X_{11,X_3}} &= \frac{\partial X_{11}}{\partial X_3} \\ \overline{X_{22,X_1}} &= \frac{\partial X_{22}}{\partial X_1}; & \overline{X_{22,X_2}} &= \frac{\partial X_{22}}{\partial X_2} + \frac{X_{33}}{R_{X_2}}; \\ \overline{X_{22,X_3}} &= \frac{\partial X_{22}}{\partial X_3}; & \overline{X_{33,X_1}} &= \frac{\partial X_{33}}{\partial X_1} - \frac{X_{11}}{R_{X_1}}; \\ \overline{X_{33,X_2}} &= \frac{\partial X_{33}}{\partial X_2} - \frac{X_{22}}{R_{X_2}} \end{aligned}$$

Now, the linear strain tensor is

$$\{\varepsilon_l\} = \begin{Bmatrix} \varepsilon_{X_1}^0 \\ \varepsilon_{X_2}^0 \\ \varepsilon_{X_1 X_2}^0 \\ \varepsilon_{X_1 X_3}^0 \\ \varepsilon_{X_2 X_3}^0 \end{Bmatrix} + X_3 \begin{Bmatrix} k_{X_1}^1 \\ k_{X_2}^1 \\ k_{X_1 X_2}^1 \\ k_{X_1 X_3}^1 \\ k_{X_2 X_3}^1 \end{Bmatrix} + X_3^2 \begin{Bmatrix} k_{X_1}^2 \\ k_{X_2}^2 \\ k_{X_1 X_2}^2 \\ k_{X_1 X_3}^2 \\ k_{X_2 X_3}^2 \end{Bmatrix} + X_3^3 \begin{Bmatrix} k_{X_1}^3 \\ k_{X_2}^3 \\ k_{X_1 X_2}^3 \\ k_{X_1 X_3}^3 \\ k_{X_2 X_3}^3 \end{Bmatrix} \quad (15)$$

or

$$\{\varepsilon_l\} = [T_l]\{\overline{\varepsilon}_l\} = \{\varepsilon^0\} + X_3\{k^1\} + X_3^2\{k^2\} + X_3^3\{k^3\} \quad (16)$$

where, $\{\overline{\varepsilon}_l\}_{20 \times 1}$ and $[T_l]_{5 \times 20}$ are the mid-plane strain terms matrix and linear thickness coordinate, respectively.

2.2.2 Finite element formulation

For the modelling purpose, a nine noded isoparametric quadrilateral Lagrangian element with nine degrees of freedom (DOF) per node is used for the discretization of the present model. The finite element presentation of the mid-plane displacement vector using the shape function $[N]$ is given below in Eq. (17) (Cook *et al.* 2009).

$$\{\delta_0\} = \sum_{i=1}^9 [N] \{\delta_{0i}\} \quad (17)$$

where, $[N]$ is nodal shape function, $\{\delta_{0i}\}$ is the mid-plane displacement vector for the i^{th} node and is given by

$$\{\delta_{0i}\} = \{X_{110_i} X_{220_i} X_{330_i} \psi_{x_i} \psi_{y_i} X_{110_i}^* X_{220_i}^* \psi_{x_i}^* \psi_{y_i}^*\}^T$$

Now, the mid-plane strain term is written as

$$\{\overline{\varepsilon}_l\} = [B]\{\delta_{0i}\} \quad (18)$$

where, $[B]_{20 \times 9}$ is the product of shape functions and the differential operators.

2.2.3 Stress-strain relation

The generic form of the constitutive relations for the FGM structural component expressed as (Kar and Panda 2016)

$$\{\sigma\} = \begin{Bmatrix} \sigma_{X_1 X_1} \\ \sigma_{X_2 X_2} \\ \tau_{X_1 X_2} \\ \tau_{X_1 X_3} \\ \tau_{X_2 X_3} \end{Bmatrix} = \begin{bmatrix} E & E \times \mu & 0 & 0 & 0 \\ \frac{1-\mu^2}{E \times \mu} & \frac{1-\mu^2}{E} & 0 & 0 & 0 \\ 0 & 0 & \frac{E}{2(1+\mu)} & 0 & 0 \\ 0 & 0 & 0 & \frac{E}{2(1+\mu)} & 0 \\ 0 & 0 & 0 & 0 & \frac{E}{2(1+\mu)} \end{bmatrix} \begin{Bmatrix} \varepsilon_{X_1 X_1} \\ \varepsilon_{X_2 X_2} \\ \gamma_{X_1 X_2} \\ \gamma_{X_1 X_3} \\ \gamma_{X_2 X_3} \end{Bmatrix} = [Q]\{\varepsilon\} \quad (19)$$

where, $\{\sigma\}$ and $\{\varepsilon\}$ are the stress and the strain vectors, respectively and $[Q]$ is the reduced stiffness matrix.

Now, the strain energy of the FG structure is written as

$$U = 0.5 \times \int_v \{\varepsilon\}^T \{\sigma\} dV \quad (20)$$

Further, the energy functional can be rewritten by utilizing the corresponding stress and strain terms in the Eq. (20) and conceded to the following form.

$$U = 0.5 \times \int_A (\{\overline{\varepsilon}_l\}^T [D] \{\overline{\varepsilon}_l\}) dA \quad (21)$$

where

$$[D] = \int_{-h/2}^{h/2} [T_l]^T [Q] [T_l] dX_3$$

Now, the kinetic energy of the FG structure can be expressed as

$$T = 0.5 \int_v \rho \{\delta\}^T \{\dot{\delta}\} dV \quad (22)$$

$$\begin{aligned} T &= 0.5 \times \int_A \left(\int_{-0.5h}^{0.5h} \{\delta_0\}^T [f]^T \rho [f] \{\dot{\delta}_0\} dX_3 \right) dA \\ &= 0.5 \times \int_A \{\delta_0\}^T [m] \{\dot{\delta}_0\} dA \end{aligned} \quad (23)$$

where, ρ , $\{\delta\}$ and $[m]$ are the mass density, velocity vector and elemental inertia matrix, respectively and

$$[m] = \int_{-h/2}^{h/2} [f]^T \rho [f] dX_3$$

2.2.4 Governing equations

In this subsection, the governing equation for the vibration study can be presented in Eq. (24) as

$$\delta \int_{t_1}^{t_2} L dt = \int_{t_1}^{t_2} (T - U) dt = 0 \tag{24}$$

Finally, the eigenvalue type equation is derived using the Eqs. (20) and (24).

$$[M]\{\ddot{\delta}\} + [K]\{\delta\} = 0 \tag{25}$$

$$([K] - \omega^2[M])\{\delta\} = 0 \tag{26}$$

where, ω , $[K]$ and $[M]$ are the natural frequency, system stiffness matrix and global mass matrix of the FG panel and

$$[M] = \int_A [N]^T [m][N] dA$$

Finally, the required responses can be obtained by solving Eq. (26).

3. Results and discussions

After the successful development of the proposed higher-order finite element formulation, a customized compute code has been prepared considering the linear stiffness matrix only in the MATLAB environment. Subsequently, the free vibration frequency of the graded structure evaluated computationally for the different design parameters i.e., thickness ratio (S), aspect ratio (O), curvature ratio (R/h), power-law exponent (n), porosity index (λ). For the computational calculation, the necessary FG elastic properties (Table 1) of the material constituents adopted as per the requirements.

3.1 Validation and convergence study

Now, to establish the currently proposed higher-order FE model, few examples as same as the reference are

studied in this subsection. In general, the accuracy of any numerical solution depends on its convergence and validity. In this regard, the non-dimensional natural frequencies of the FG structures consists of various grading pattern (P-FGM, S-FGM and E-FGM) and geometrical configurations (spherical and plate) are evaluated considering the linear stiffness only. The present and the reference data (Amir and Talha 2019) are computed for the different element sizes along with the corresponding directions including the comparison presented in Fig. 6. The data points indicate the converging pattern when the mesh sizes increase from the coarse to fine. The responses of a SSSS P-FGM ($Al_2O_3/SUS304$) spherical panel ($O = 1, S = 100$ and $n = 0, 0.6, 1, 2, 5, \infty$) has been solved for the comparison purpose. It is observed from Fig. 6 that the differences between the results are too small i.e., within 0.80 to 1.05 % for all the values of a power-law exponent.

Further, to show the capability of the current model, two more examples are solved for two different grading patterns (S-FGM and E-FGM) and support conditions (SSSS and clamped i.e., CCCC). The responses are obtained using the same geometrical and material parameters as in the references (Han *et al.* 2008 and Chakraverty and Pradhan 2014). The frequencies are obtained for the first three and five modes and presented in Tables 2-3, respectively and it is observed that the variation between the result is not very large i.e., within 0.24 to 3.21 % for S-FGM and 5.92 to 8.51 % for E-FGM. The difference between the results of E-FGM is more as compare to P-FGM and S-FGM. This is because the frequency values are calculated for E-FGM are

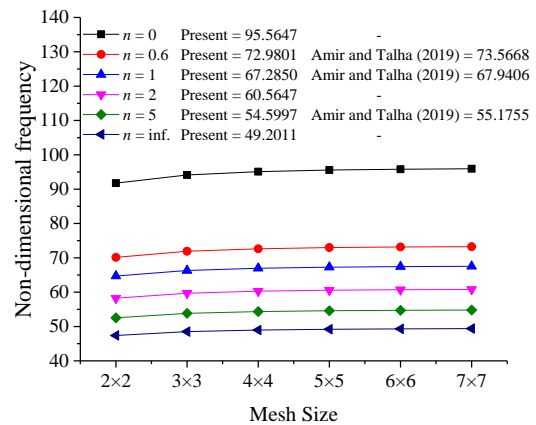


Fig. 6 Convergence and validation study of P-FGM

Table 1 Material properties

Material	Properties			
	Modulus of elasticity (E) (GPa)	Poisson's ratio (μ)	Density (ρ) (kg/m ³)	
Ceramic	Alumina (Al_2O_3)	349.55	0.24	3800
	Silicon nitrate (Si_3N_4)	322.27	0.28	2370
	Zirconia (ZrO_2)	151	0.3	3000
Metal	Stainless steel ($SUS304$)	201.04	0.3262	8166
	Aluminium (Al)	70	0.3	2707

Table 2 Frequency (non-dimensional) of SSSS square S-FGM plate ($S = 100, O = 1$)

Power-law exponent (n)	Han <i>et al.</i> (2008)			Present		
	1	2	3	1	2	3
0	9.041	22.705	22.705	9.0646	23.4603	23.4604
1	7.555	18.992	18.993	7.5789	19.6165	19.6166
2	7.457	18.745	18.747	7.4784	19.3572	19.3572
5	7.373	18.533	18.535	7.3919	19.1338	19.1339
10	7.348	18.47	18.472	7.3661	19.0672	19.0672
∞	6.148	15.459	15.459	6.1718	15.9733	15.9733

Table 3 Frequency parameters of CCCC E-FGM plate ($S = 100$)

Aspect ratio (O)	Chakraverty and Pradhan (2014)					Present				
	1	2	3	4	5	1	2	3	4	5
0.2	15.024	15.559	16.514	17.949	20.456	16.066	16.648	17.699	19.326	21.667
0.5	16.316	21.129	29.752	42.217	42.475	17.447	22.678	32.262	45.810	46.483
1	23.89	48.724	48.724	71.868	87.556	25.527	52.421	52.421	77.279	95.101
2	65.265	84.515	119.01	168.87	169.9	69.414	90.167	127.98	181.05	183.67
2.5	98.099	115.38	147.06	194.24	261.74	104.06	122.61	157.23	209.82	277.28

Table 4 Effect of aspect ratio, power-law exponent, porosity index and porosity distribution on the frequency data of SSSS P-FGM spherical panel ($S = 100$)

Power-law exponent (n)	Aspect ratio (O)	Porosity index (λ) and distribution					
		Even			Uneven		
		0	0.1	0.2	0	0.1	0.2
1	0.2	26.4674	26.7412	27.0266	26.4674	26.6015	26.7343
	0.5	64.3875	64.4818	64.5748	64.3875	64.4495	64.5176
	1	67.2850	67.3851	67.4825	67.2850	67.3409	67.3989
	3	72.4671	72.4320	72.3943	72.4671	72.5446	72.6322
	5	87.4184	87.0889	86.7554	87.4184	87.7674	88.1581
5	0.2	21.2774	21.0018	20.6149	21.2774	21.1464	20.9874
	0.5	52.2579	51.1517	49.7732	52.2579	51.7408	51.1680
	1	54.5997	53.4360	51.9883	54.5997	54.0471	53.4355
	3	59.1441	57.7803	56.1192	59.1441	58.5808	57.9636
	5	72.4165	70.5985	68.4514	72.4165	72.0336	71.6199

based on Classical plate theory (three degrees of freedom) whereas the present data is obtained using HSDT kinematics (nine degrees of freedom).

3.2 Vibration analysis of FGM

After successful completion of the validation study, the vibration behaviour of all three types of FG structure is discussed in this section for different influencing parameters like aspect ratio, thickness ratio, power-law exponent, type of porosity, porosity index, boundary conditions and geometries. In this analysis, Alumina and Stainless steel are taken as ceramic and metal constituents, respectively. The material properties for the calculation purpose are taken as in Table 1. The linear frequencies are made a non-dimensional form using the given formula in

the following line. The non-dimensional form of presentation majorly helps in understanding the effect of a particular structural parameter on the frequency behaviour.

$$\bar{\omega} = \frac{\omega a^2}{h} \sqrt{\frac{\rho_c}{E_c}}$$

where, ω is the natural frequency of the FG structure, E_c and ρ_c are the modulus of elasticity and density of the ceramic constituent.

Table 5 Natural frequency of P-FGM spherical panel for various boundary condition. ($S = 100, O = 2, n = 5$)

Boundary condition	Porosity index (λ) and distribution					
	Even			Uneven		
	0	0.1	0.2	0	0.1	0.2
SSSS	56.8153	55.546	53.985	56.8153	56.2305	55.5877
CCCC	71.7804	69.7211	67.3398	71.7804	70.9475	70.0727
CFFF	1.1268	1.1061	1.08	1.1268	1.1263	1.1254

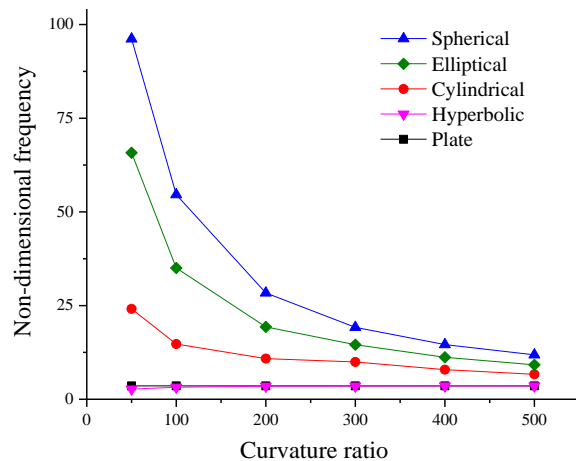


Fig. 7 Natural frequency of SSSS P-FGM structure for different geometry and curvature ratio

Table 6 Effect of porosity index, porosity distribution, aspect ratio and power-law exponent on the frequency parameter of SSSS spherical S-FGM panel ($S = 100$)

Power-law exponent (n)	Aspect ratio (O)	Porosity index (λ) and distribution					
		Even			Uneven		
		0	0.1	0.2	0	0.1	0.2
1	0.2	26.4674	26.7412	27.0266	26.4674	26.6015	26.7343
	0.5	64.3845	64.4818	64.5748	64.3845	64.4495	64.5176
	1	67.2850	67.3851	67.4825	67.2850	67.3409	67.3989
	3	72.4671	72.4320	72.3943	72.4671	72.5446	72.6322
	5	87.4184	87.0889	86.7554	87.4184	87.7674	88.1581
5	0.2	26.5322	26.8142	27.1100	26.5322	26.6702	26.8074
	0.5	64.3528	64.4434	64.5274	64.3528	64.4160	64.4821
	1	67.2543	67.3527	67.4478	67.2543	67.3098	67.3672
	3	72.1952	72.1482	72.0928	72.1952	72.2678	72.3489
	5	86.5839	86.1713	85.7193	86.5839	86.9001	87.2504

3.2.1 P-FGM

In this subsection, the influence of aspect ratio with even and uneven porosity distribution on the frequency data(non-dimensional) of FG panel is obtained with different exponent values ($n = 1$ and $n = 5$) and shown in Table 4. From the table, it is seen that the increase in aspect ratio causes an increment in the natural frequencies. Also, the even and uneven porosity results are the same when the porosity index equals to zero ($\lambda = 0$). In addition, the frequency parameters of the P-FGM structure for various boundary conditions are given in Table 5. From the table, it

Table 7 Effect of boundary condition on the frequency parameter of SSSS S-FGM spherical panel ($S = 100, O = 2, n = 5$)

Boundary condition	Porosity index (λ) and distribution					
	Even			Uneven		
	0	0.1	0.2	0	0.1	0.2
SSSS	69.7523	69.7787	69.8009	69.7523	69.7916	69.8350
CCCC	86.9367	86.3492	85.7600	86.9367	86.8167	86.7241
CFFF	1.3441	1.3435	1.3414	1.3441	1.3540	1.3647

Table 8 Effect of porosity index, porosity distribution and power-law exponent on the frequency parameter of SSSS S-FGM spherical panel ($S = 100, O = 1$)

Power-law exponent (n)	Porosity index (λ) and distribution					
	Even			Uneven		
	0	0.1	0.2	0	0.1	0.2
0	67.4268	67.5334	67.6392	67.4268	67.4857	67.5472
0.6	67.3106	67.4120	67.5111	67.3106	67.3673	67.4261
1	67.2850	67.3851	67.4825	67.2850	67.3409	67.3989
2	67.2619	67.3608	67.4566	67.2619	67.3172	67.3746
5	67.2543	67.3527	67.4478	67.2543	67.3098	67.3672
∞	67.2681	67.3669	67.4627	67.2681	67.3249	67.3840

is observed that the CCCC boundary condition give higher frequency values than the cantilever (CFFF) and SSSS conditions. Further, the influence of the curvature ratio and various geometries on the frequency parameters of the FG structure is shown in Fig. 7. It is observed from Fig. 7 that the curvature ratio affects spherical and elliptical panel most whereas the effect on the hyperbolic and plate structure is least.

3.2.2 S-FGM

Now, the frequency parameters of S-FGM spherical panel with even and uneven type of porosity distribution for various values of power-law exponent and aspect ratio are computed and presented in Table 6. Also, the frequency parameters (non-dimensional) of the S-FGM structure for different boundary conditions are presented in Table 7. Similarly, the influence of the porosity index and power-law exponent on the non-dimensional frequency parameters of S-FGM panel are obtained and shown in Table 8. Further, the consequence of curvature ratio and different geometries

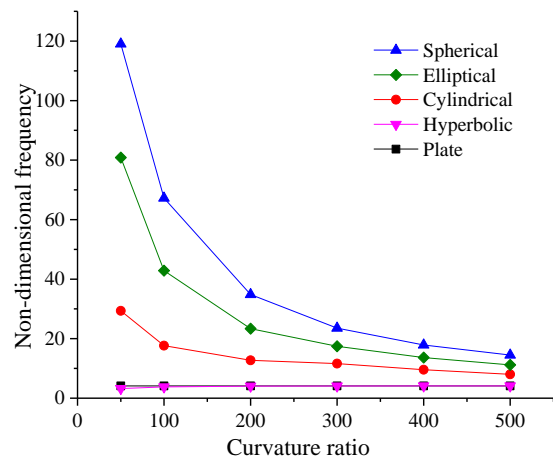


Fig. 8 Effect of curvature ratio and geometry on the natural frequency of SSSS S-FGM structure

Table 9 Natural frequencies (non-dimensional) of the SSSS E-FGM panel for different thickness and aspect ratio

Thickness ratio (S)	Aspect ratio (O)	Porosity index (λ) and distribution					
		Even			Uneven		
		0	0.1	0.2	0	0.1	0.2
5	0.2	1.3429	1.304	1.2662	1.3429	1.3199	1.2972
	0.5	3.4456	3.3465	3.2499	3.4456	3.3864	3.328
	1	4.4537	4.3097	4.1705	4.4537	4.3863	4.3197
	3	6.842	6.6454	6.4539	6.842	6.723	6.6059
	5	6.8654	6.6971	6.5039	6.8654	6.7759	6.6582
10	0.2	2.7033	2.6251	2.5488	2.7033	2.6574	2.6121
	0.5	6.749	6.5369	6.3313	6.749	6.6397	6.5319
	1	7.4454	7.2077	6.9777	7.4454	7.328	7.2123
	3	13.9593	13.5595	13.1696	13.9593	13.72	13.4843
	5	13.9731	13.5728	13.1826	13.9731	13.7334	13.4975
100	0.2	26.784	26.0067	25.2495	26.784	26.331	25.8849
	0.5	65.111	63.0389	61.7751	65.111	64.0506	63.0056
	1	68.0403	65.8739	63.7751	68.0403	66.9301	65.8363
	3	73.2954	70.9306	68.6423	73.2954	72.1196	70.9606
	5	88.5245	85.6058	82.7891	88.5245	87.1916	85.8762

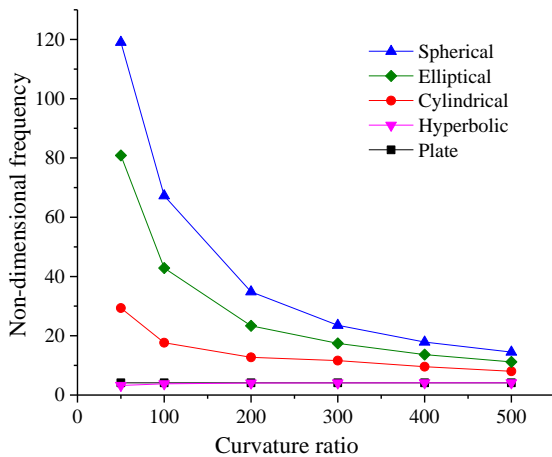


Fig. 9 Non-dimensional frequency of SSSS E-FGM structure for different geometry and curvature ratio

on the non-dimensional frequency parameter of the S-FGM structure with SSSS end condition is shown in Fig. 8.

3.2.3 E-FGM

The influence of porosity index, porosity distribution, thickness and aspect ratio on the linear eigenvalues of simply supported spherical E-FGM panel are obtained by utilizing the present higher-order model and presented in Table 9. The tabulated data indicate that the eigenvalues are following an ascending order while both the thickness ratio and aspect ratio of the panel component increases. Also, the effect of curvature ratio and various geometries on the frequency parameters of the E-FGM panel is shown in Fig. 9.

4. Conclusions

The current study is proposed to develop the higher-order FE model for the FG structures, including different type of porosity distribution (even and uneven) and grading patterns. The model applicability has been established by computing the vibration responses numerically via homemade computer code (MATLAB environment) with the help of mathematical formulation. The necessary validity of the model is presented by matching the present results with that of published data. The convergence and subsequent validation study indicate the suitability of the proposed higher-order FE model for the FG structures with and without porosity effect. The important outcomes of the present work are listed below:

- The porosity index causes a variation in frequency parameters by 0.4% to 7% whereas the deviation can be noted in between 0.5% to 3.6% depending upon other influential parameters.
- Sigmoid distribution method gives more stable frequency data in comparison to the power-law and exponentially distributed FG structure.
- The frequencies are same for P and S type of FG structures while the exponent values approaches unity i.e., $n = 1$.
- Also, the linear frequency results are vary consistently with the variation of the structural design associated parameters i.e., thickness ratios, aspect ratios, power-law exponents, porosity indices, grading patterns and geometrical configurations.

References

- Amir, M. and Talha, M. (2019), "Nonlinear vibration characteristics of shear deformable functionally graded curved panels with porosity including temperature effects", *Int. J. Press. Vessel Pip.*, **172**, 28-41.
<https://doi.org/10.1016/j.ijpvp.2019.03.008>
- Amnieh, H.B., Zamzam, M.S. and Kolahchi, R. (2018), "Dynamic analysis of non-homogeneous concrete blocks mixed by SiO₂ nanoparticles subjected to blast load experimentally and theoretically", *Constr. Build. Mater.*, **174**, 633-644.
<https://doi.org/10.1016/j.conbuildmat.2018.04.140>
- Arani, A.G. and Kolahchi, R. (2016), "Nonlinear vibration analysis of piezoelectric plates reinforced with carbon nanotubes using DQM", *Smart Struct. Syst., Int. J.*, **18**(4), 787-800.
<https://doi.org/10.12989/sss.2016.18.4.787>
- Asadi, H., Aghdam, M.M. and Shakeri, M. (2014), "Vibration analysis of axially moving line supported functionally graded plates with temperature-dependent properties", *J. Mech. Eng. Sci.*, **228**(6), 953-969.
<https://doi.org/10.1177/0954406213498033>
- Atmane, H.A., Tounsi, A., Mechab, I. and Bedia, E.A.A. (2010), "Free vibration analysis of functionally graded plates resting on Winkler-Pasternak elastic foundations using a new shear deformation theory", *Int. J. Mech. Mater. Des.*, **6**(2), 113-121.
<https://doi.org/10.1007/s10999-010-9110-x>
- Avcar, M. (2019), "Free vibration of imperfect sigmoid and power law functionally graded beams", *Steel Compos. Struct., Int. J.*, **30**(6), 603-615. <https://doi.org/10.12989/scs.2019.30.6.603>
- Barati, M.R. and Zenkour, A.M. (2018), "Vibration analysis of functionally graded graphene platelet reinforced cylindrical shells with different porosity distributions", *Mech. Adv. Mater. Struct.*, **26**(18), 1580-1588.
<https://doi.org/10.1080/15376494.2018.1444235>
- Belkorissat, I., Sid, M., Houari, A., Tounsi, A., Bedia, E.A.A. and Mahmoud, S.R. (2015), "On vibration properties of functionally graded nano-plate using a new nonlocal refined four variable model", *Steel Compos. Struct., Int. J.*, **18**(4), 1063-1081.
<https://doi.org/10.12989/scs.2015.18.4.1063>
- Bohra, P., Sharma, P., Bhandari, M., Bohra, S. and Prakash, V. (2017), "Free vibration response of functionally graded material plate subjected to simply supported and simply supported-clamped boundary conditions", *Int. J. Res. Appl. Sci. Eng. Tech.*, **5**(XII), 501-527.
- Chakraverty, S. and Pradhan, K.K. (2014), "Free vibration of exponential functionally graded rectangular plates in thermal environment with general boundary conditions", *Aerosp. Sci. Tech.*, **36**, 132-156. <https://doi.org/10.1016/j.ast.2014.04.005>
- Chi, S.-H. and Chung, Y.-L. (2006), "Mechanical behavior of functionally graded material plates under transverse load — Part I: Analysis", *Int. J. Solids Struct.*, **43**, 3657-3674.
<https://doi.org/10.1016/j.ijsolstr.2005.04.011>
- Cook, R.D., Malkus, D.S., Plesha, M.E. and Witt, R.J. (2009), *Concepts and Applications of Finite Element Analysis*, (4th Edition), John Wiley & Sons, Singapore.
- Ghannad, M. and Gharooni, H. (2012), "Displacements and stresses in pressurized thick FGM cylinders with varying properties of power function based on HSDT", *J. Solid Mech.*, **4**(3), 237-251.
- Ghannadpour, S.A.M., Mohammadi, B. and Fazilati, J. (2013), "Bending, buckling and vibration problems of nonlocal Euler beams using Ritz method", *Comp. Struct.*, **96**, 584-589.
<https://doi.org/10.1016/j.compstruct.2012.08.024>
- Ghassabi, A.A., Dag, S. and Cigeroglu, E. (2017), "Free vibration analysis of functionally graded rectangular nanoplates considering spatial variation of the nonlocal parameter", *Arch. Mech.*, **69**(2), 105-130.
- Hajmohammad, M.H., Zarei, M.S., Farrokhanian, A. and Kolahchi, R. (2018), "A layerwise theory for buckling analysis of truncated conical shells reinforced by CNTs and carbon fibers integrated with piezoelectric layers in hygrothermal environment", *Adv. Nano. Res., Int. J.*, **6**(4), 299-321.
<https://doi.org/10.12989/anr.2018.6.4.299>
- Han, S.-C., Lomboy, G.R. and Kim, K.-D. (2008), "Mechanical vibration and buckling analysis of FGM plates and shells using a four-node Quasi-Conforming shell element", *Int. J. Struct. Stab. Dyn.*, **8**(2), 203-229.
<https://doi.org/10.1142/s0219455408002624>
- Hebali, H., Tounsi, A., Sid, M.H.A., Bessaim, A. and Bedia, A.E.A. (2014), "New Quasi-3D hyperbolic shear deformation theory for the static and free vibration analysis of functionally graded plates", *J. Eng. Mech.*, **140**(2), 374-383.
[https://doi.org/10.1061/\(ASCE\)EM.1943-7889.0000665](https://doi.org/10.1061/(ASCE)EM.1943-7889.0000665)
- Huang, C.S., McGee, I.O.G. and Chang, M.J. (2011), "Vibrations of cracked rectangular FGM thick plates", *Comp. Struct.*, **93**, 1747-1764. <https://doi.org/10.1016/j.compstruct.2011.01.005>
- Jamaludin, S.N.S., Mustapha, F., Nuruzzaman, D.M. and Basri, S.N. (2013), "A review on the fabrication techniques of functionally graded ceramic-metallic materials in advanced composites", *Sci. Res. Essays*, **8**(21), 828-840.
<https://doi.org/10.5897/SRE2012.0743>
- Jassas, M.R., Bidgoli, M.R. and Kolahchi, R. (2019), "Forced vibration analysis of concrete slabs reinforced by agglomerated SiO₂ nanoparticles based on numerical methods", *Constr. Build. Mater.*, **211**, 796-806.
<https://doi.org/10.1016/j.conbuildmat.2019.03.263>
- Jouneghani, Z.F., Dimitri, R., Bacciocchi, M. and Tornabene, F. (2017), "Free vibration analysis of functionally graded porous doubly-curved shells based on the first-order shear deformation theory", *Appl. Sci.*, **7**(12), 1-20.
<https://doi.org/10.3390/app7121252>
- Kar, V.R. and Panda, S.K. (2016), "Nonlinear free vibration of functionally graded doubly curved shear deformable panels using finite element method", *J. Vib. Control*, **22**(7), 1935-1949.
<https://doi.org/10.1177/1077546314545102>
- Kiani, Y., Dimitri, R. and Tornabene, F. (2018), "Free vibration of FG-CNT reinforced composite skew cylindrical shells using the Chebyshev-Ritz formulation", *Comp. Part B*, **147**, 169-177.
<https://doi.org/10.1016/j.compositesb.2018.04.028>
- Kim, J. and Reddy, J.N. (2013), "Analytical solutions for bending, vibration and buckling of FGM plates using a couple stress-based third-order theory", *Comp. Struct.*, **103**, 86-98.
<https://doi.org/10.1016/j.compstruct.2013.03.007>
- Kolahchi, R., Hosseini, H., Fakhari, M.H., Taherifar, R. and Mahmoudi, M. (2019), "A numerical method for magneto-hygro-thermal postbuckling analysis of defective quadrilateral graphene sheets using higher order nonlocal strain gradient theory with different movable boundary conditions", *Comput. Math. with Appl.*, **78**, 2018-2034.
<https://doi.org/10.1016/j.camwa.2019.03.042>
- Liu, S., Yu, T. and Bui, T.Q. (2017), "Size effects of functionally graded moderately thick microplates: A novel non-classical simple-FSDT isogeometric analysis", *Eur. J. Mech. / A Solids*, **66**, 446-458. <https://doi.org/10.1016/j.euromechsol.2017.08.008>
- Mashat, D.S., Carrera, E., Zenkour, A.M., Khatteeb, S.A.A. and Filippi, M. (2014), "Free vibration of FGM layered beams by various theories and finite elements", *Compos. Part B*, **59**, 269-278. <https://doi.org/10.1016/j.compositesb.2013.12.008>
- Meiche, N.E., Tounsi, A., Ziane, N., Mechab, I. and Bedia, E.A.A. (2011), "A new hyperbolic shear deformation theory for buckling and vibration of functionally graded sandwich plate", *Int. J. Mech. Sci.*, **53**(4), 237-247.
<https://doi.org/10.1016/j.ijmecsci.2011.01.004>
- Mirzaei, M. and Kiani, Y. (2017), "Nonlinear free vibration of FG-

- CNT reinforced composite plates”, *Struct. Eng. Mech., Int. J.*, **64**(3), 381-390. <https://doi.org/10.12989/sem.2017.64.3.381>
- Mohammadi, B. and Ghannadpour, S.A.M. (2011), “Energy approach vibration analysis of nonlocal Timoshenko beam theory”, *Procedia Eng.*, **10**, 1766-1771. <https://doi.org/10.1016/j.proeng.2011.04.294>
- Ramu, I. and Mohanty, S.C. (2014), “Modal Analysis of Functionally Graded Material Plates Using Finite Element Method”. *Procedia Mater. Sci.*, **6**, 460-467. <https://doi.org/10.1016/j.mspro.2014.07.059>
- Reddy, J.N. (2004), *Mechanics of Laminated Composite — Plates and Shells — Theory and Analysis*, (2nd Edition) CRC Press, Boca Raton, FL, USA.
- Shahverdi, H. and Barati, M.R. (2017), “Vibration analysis of porous functionally graded nanoplates”, *Int. J. Eng. Sci.*, **120**, 82-99. <https://doi.org/10.1016/j.ijengsci.2017.06.008>
- Sheikh, A.H., Asadi, A. and Thomsen, O.T. (2015), “Vibration of thin-walled laminated composite beams having open and closed sections”, *Compos. Struct.*, **134**, 209-215. <https://doi.org/10.1016/j.compstruct.2015.08.025>
- Talha, M. and Singh, B.N. (2010), “Static response and free vibration analysis of FGM plates using higher order shear deformation theory”, *Appl. Math. Model.*, **34**, 3991-4011. <https://doi.org/10.1016/j.apm.2010.03.034>
- Thai, H.T. and Choi, D.-H. (2013), “A simple first-order shear deformation theory for the bending and free vibration analysis of functionally graded plates”, *Comp. Struct.*, **101**, 332-340. <https://doi.org/10.1016/j.compstruct.2013.02.019>
- Tornabene, F. (2009), “Free vibration analysis of functionally graded conical, cylindrical shell and annular plate structures with a four-parameter power-law distribution”, *Comput. Methods. Appl. Mech. Eng.*, **198**, 2911-2935. <https://doi.org/10.1016/j.cma.2009.04.011>
- Vu, T.-V., Nguyen, N.-H., Khosravifard, A., Hematiyan, M.R., Tanaka, S. and Bui, T.Q. (2017), “A simple FSDT-based meshfree method for analysis of functionally graded plates”, *Eng. Anal. Bound. Elem.*, **79**, 1-12. <https://doi.org/10.1016/j.enganabound.2017.03.002>
- Vu, T.-V., Khosravifard, A., Hematiyan, M.R. and Bui, T.Q. (2019), “Enhanced meshfree method with new correlation functions for functionally graded plates using a refined inverse sin shear deformation plate theory”, *Eur. J. Mech. / A Solids*, **74**, 160-175. <https://doi.org/10.1016/j.euromechsol.2018.11.005>
- Wang, Y.Q. and Zu, J.W. (2017), “Vibration behaviors of functionally graded rectangular plates with porosities and moving in thermal environment”, *Aerosp. Sci. Tech.*, **69**, 550-562. <https://doi.org/10.1016/j.ast.2017.07.023>
- Wang, Y.Q. and Zu, J.W. (2018), “Vibration characteristics of moving sigmoid functionally graded plates containing porosities”. *Int. J. Mech. Mater. Des.*, **14**, 473-489. <https://doi.org/10.1007/s10999-017-9385-2>
- Wattanasakulpong, N., Prusty, B.G., Kelly, D.W. and Hoffman, M. (2012), “Free vibration analysis of layered functionally graded beams with experimental validation”, *Mater. Des.*, **36**, 182-190. <https://doi.org/10.1016/j.matdes.2011.10.049>